

Balanced 3DGS: Gaussian-wise Parallelism Rendering with Fine-Grained Tiling

Hao Gui¹ Lin Hu² Rui Chen² Mingxiao Huang¹

Yuxin Yin¹ Jin Yang¹ Yong Wu¹

¹ Li Auto, Shanghai, China ² NVIDIA, Beijing, China

Abstract

3D Gaussian Splatting (3DGS) is increasingly attracting attention in both academia and industry owing to its superior visual quality and rendering speed. However, training a 3DGS model remains a time-intensive task, especially in load imbalance scenarios where workload diversity among pixels and Gaussian spheres causes poor renderCUDA kernel performance. We introduce Balanced 3DGS, a Gaussian-wise parallelism rendering with fine-grained tiling approach in 3DGS training process, perfectly solving load-imbalance issues. First, we innovatively introduce the inter-block dynamic workload distribution technique to map workloads to Streaming Multiprocessor(SM) resources within a single GPU dynamically, which constitutes the foundation of load balancing. Second, we are the first to propose the Gaussian-wise parallel rendering technique to significantly reduce workload divergence inside a warp, which serves as a critical component in addressing load imbalance. Based on the above two methods, we further creatively put forward the fine-grained combined load balancing technique to uniformly distribute workload across all SMs, which boosts the forward renderCUDA kernel performance by up to 7.52x. Besides, we present a self-adaptive render kernel selection strategy during the 3DGS training process based on different load-balance situations, which effectively improves training efficiency.

1. Introduction

3DGS [24] is an innovative technique in 3D graphics that facilitates the reconstruction of detailed 3D scenes from images and viewpoints, allowing real-time multi-angle rendering. While it holds great promise, it also encounters significant computational challenges, which underscores the necessity for optimization [2, 6, 16, 53]. To boost 3DGS performance, two primary optimization strategies are currently being explored. The first strategy focuses on the

modification of the algorithm itself to achieve better precision, fewer storage, or higher computational efficiency [1, 4, 8, 22, 27, 30, 31, 33, 37, 45, 46]. The second strategy, rather than making modifications to the algorithm itself, aims to enhance computational efficiency of raw algorithm by means of a variety of strategies, such as the implementation of intelligent task scheduling or the optimization of CUDA kernels [13, 15, 18, 35, 50, 53].

Despite great advancements in 3DGS technology, training a 3DGS model remains a challenging and time-consuming task, particularly when faced with load imbalance situations. In such cases, imbalanced workload between pixels and Gaussian spheres can hinder training performance. Specifically, graphics processors (GPUs) are designed to handle regular and homogeneous tasks, and threads on GPUs run in SIMT (Single Instruction Multiple Threads) manner. Therefore, discrepancies in workload between pixels and Gaussian spheres can result in some threads being active while others remain idle, thereby degrading overall performance. To the best of our knowledge, we are the first to address those imbalance issues in kernel level. Through in-depth analysis and experimentation during the 3DGS training process, we have identified and characterized three significant load imbalance problems, which are as follows:

Load imbalance on SMs due to CUDA’s static distribution: there is a load imbalance issue on SMs if we use static distribution. The renderCUDA dispatches tasks to SMs statically based on image and thread block size. Although the number of thread block tasks among different SMs is the same, the workload of each thread block can vary widely. This is a performance factor that has been neglected and results in a load imbalance between SMs.

Load imbalance in tiles: there is an issue of load imbalance among tiles. In 3DGS, the image is initially divided into multiple non-overlapping tiles to avoid the cost of deriving Gaussians for each pixel. Each tile contains

16×16 pixels as the existing method [24]. However, some tiles may have extreme workloads compared with other light-workload tiles, if the basic CUDA distribution and tiling strategy remain unchanged, a severe load imbalance among SMs will occur.

Load imbalance across training stages: During the 3DGS training, the data characteristics change remarkably in different phases. At the initial stage, metrics such as Gaussian distribution have significant differences among various blocks or threads. As the training progresses, these imbalances get improved as data characteristics change. After numerous iterations, extreme data metrics become more balanced.

To address these issues comprehensively, we introduce "Balanced 3DGS". The highlights include: We are the first to propose the Gaussian-based parallel load balancing method to optimize the forward computation of the render CUDA kernel within warps. Additionally, we innovatively present inter-block dynamic workload distribution to boost the performance of the forward of render CUDA kernel. By evenly distributing tasks among computation blocks, it minimizes idle time of threads and maximizes resource utilization. Our fine-grained combined load balancing approach combines these two techniques, providing a complete solution to load imbalance problems. We propose an experiment-based adaptive kernel selection strategy. This strategy overcomes the limitations of manual metric selection, presents a more accurate reflection of training process, and ensures better performance and efficiency.

2. Background

2.1. 3DGS

The 3D Gaussian can be mathematically expressed as:

$$G(x) = e^{-\frac{1}{2}(x-\mu)^T \Sigma^{-1}(x-\mu)} \quad (1)$$

where x represents an arbitrary position within the 3D scene. Each 3D Gaussian splat is allocated a position (mean μ), and Σ represents the covariance matrix of the 3D Gaussian function, and it is a positive definite matrix.

The Gaussian splatting method utilizes splatting techniques to project the 3D Gaussians onto 2D image planes for the purpose of rendering. Given the viewing transformation W and the Jacobian of the affine approximation for the projective transformation J , the covariance matrix Σ' in camera coordinates can be computed as below:

$$\Sigma' = JW \Sigma W^T J^T \quad (2)$$

Then 3D Gaussian $G(x)$ is transformed to 2D Gaussian $G'(x)$ as below:

$$G'(x) = e^{-\frac{1}{2}(x-\mu)^T \Sigma'^{-1}(x-\mu)} \quad (3)$$

Each 3D Gaussian is composed of its position, color represented by spherical harmonics, opacity, rotation, and scaling. For a given pixel, the color blending of N-sorted 2D Gaussians is determined by:

$$C = \sum_{i \in N} c_i \alpha_i \prod_{j=1}^{i-1} (1 - \alpha_j) \quad (4)$$

where c_i designates the learned color of a pixel and α_i designates the multiplication result of an opacity and its 2D Gaussian $G'(x)$.

2.2. CUDA Related

This subsection presents an in-depth introduction to GPU architecture and CUDA, a parallel computing platform and programming model developed by NVIDIA, including many key concepts that will be used in this paper such as thread, warp, block, shared memory and SM, as shown in Fig. 1.

These concepts are fundamental to understanding how parallel computing is achieved and optimized on NVIDIA GPUs, enabling developers to harness the immense computational power of these devices for a wide range of applications including scientific computing, computer graphics, and machine learning.

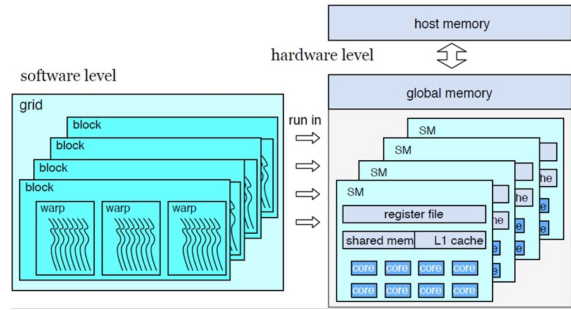


Figure 1. GPU Architecture.

Thread: a thread in the CUDA context is the basic unit of execution. It represents an independent sequence of instructions that can be executed in parallel with other threads. Each thread has its own program counter, register set, and local memory. Different threads can be used to process different tasks.

Warp: a warp is a key concept in the execution model of modern GPUs. A warp usually consists 32 threads, and those threads run in SIMT manner. This means that all the threads in a warp execute the same instruction simultaneously, but they may operate on different data. If threads

within a warp diverge in their execution paths (due to conditional statements, for example), the GPU may serialize the execution of those diverging paths to ensure correct results, but this serialization will cause severe performance drop. Thus, we should avoid thread divergence as much as we can.

Block: A block is a collection of threads that share a certain level of resources. The threads within a block have the ability to communicate and synchronize with each other through shared memory and synchronization primitives. Shared memory allows for fast data sharing among threads in the same block, which is beneficial for tasks that require data sharing and cooperation, such as parallel reduction operations. Multiple blocks are organized to a grid.

Shared Memory: shared memory is a type of memory that is accessible to all threads within a block. It allows for fast communication and data sharing among the threads in a block. Shared memory is much faster than global memory, and it is common sense that proper use of shared memory can lead to significant performance improvements.

SM: SM is a major hardware component of the GPU architecture. It contains multiple CUDA cores, along with other resources such as register files, shared memory, and cache. When a CUDA program is launched, thread blocks are mapped to SMs, and the SMs then manage the execution of the threads within those blocks. Note that one block can only be mapped one SM, but one SM can have multiple blocks. The performance of the GPU is closely related to the efficiency of the SMs in handling workload.

3. Related Works

3D Gaussian Splatting [24] has emerged as one of the most prominent novel view synthesis (NVS) and rendering techniques [5, 14, 21, 26] through the use of 3D Gaussian point cloud representations. It offers faster real-time rendering and training while maintaining high-quality output, outperforming previous NVS approaches such as NeRF [36]. Despite its advancements, the rendering efficiency of 3D Gaussian Splatting remains a critical area for improvement, particularly as the image scales increase. Ensuring efficient and high-quality rendering in such contexts remains a challenge [2, 6, 16]. Numerous efforts [12, 34, 41, 42, 49, 51] have focused on algorithmic optimizations, while others have explored engineering solutions to enhance performance.

Improving 3DGS Algorithms: Traditional 3D Gaussian Splatting combines the primitive-based representations and volumetric representations, but this approach often results in reliance on redundant Gaussians, leading to overfitting on training views and insufficient handling of texture deterioration [11], lighting effects [3, 20, 28] and the underlying geometric structures. To address these

challenges, Scaffold-GS [32] introduces anchor points from Structure from Motion (SfM) [43] to capture the geometric structure and optimize end-to-end training reconstruction. Similarly, the method in [1] employs a pruning strategy using a predetermined opacity threshold to remove redundant Gaussians, thereby accelerating computations. Building on Scaffold-GS, HAC [8] implements a binary hash grid to establish the inherent spatial relationships among contiguous anchor points, achieving greater size reduction than [32]. However, SfM technology often struggles with producing adequate point clouds on texture-less surfaces, which can negatively impact rendering quality and alignment. In contrast to traditional 3DGS using basic split and copy strategy, GaussianPro [10] provides a progressive propagation strategy, leveraging the prior existing geometry and multi-view stereo (MVS) technique [19, 23] to generate new spatial-oriented Gaussians for these challenging surfaces. GeoGaussian [31] also applies mathematical smoothness constraints to improve alignment in the textureless regions such as ceilings, furniture and walls. Additionally, [22] develops a tailored Levenberg-Marquardt (LM) replacing the traditional ADAM optimizer, further enhancing performance. CompGS [37] introduces vector quantization techniques such as K-means, significantly reducing storage and rendering demands with minimal quality loss. Following this line of work, other techniques [27, 30, 48, 52] have been developed to refine 3DGS through strategies like learnable masks, multi-scale approaches, frequently regularization, and depth regularization, leading to improved fidelity and efficiency in dynamic scene synthesis. Technological improvements also extend to dynamic environments, with methods such as HexPlane [4] reducing training times through efficient representation using learned planar features while maintaining competitive view synthesis quality. Moreover, works like Dynamic 3D Gaussians [33] and 3DGStream [45] advance dynamic scene rendering and tracking, highlighting innovations in first-person view synthesis and 4D video editing via real-time Gaussian transformations. PhysGaussian [46] further enhances Gaussians with Newtonian dynamics, facilitating high-quality motion synthesis without traditional geometric constructs.

Accelerating 3DGS Training: Most contemporary approaches expedite training by either decreasing the number of Gaussians or improving the rasterizer. However, the exploration of training optimization within this research context remains limited. Typically, 3DGS models are trained on a single GPU and are often constrained by the memory bound [8, 9, 38, 40] or the compute bound. We found that most common examples of training optimization are built on backward-render kernels [13], with inadequate attention given to forward-kernel improvements. This imbal-

ance highlights forward-render kernel optimization as a critical bottleneck for attaining efficient end-to-end 3D Gaussian Splatting training, which forms the primary motivation for our work. In 3DGS backward propagation, atomic operations on the L2 cache cause bottlenecks during gradient computation. DISTWAR [13] addresses this by dynamically distributing these operations between SM warp and L2 atomic partitions, reducing L2 cache load and atomicAdd calls, which improves GPU throughput and training efficiency. Mini-Splatting [15] observes that the inefficient spatial locality of 3D Gaussian point clouds representation where only a small number of Gaussians affect each image tile, contributing equally to the limitation of the model performance. To address this, [15, 35] introduce the densification algorithm which reduces the unnecessary model size and [35] also shifts parallelism from a traditional per-pixel to a per-splat approach for efficient backpropagation. FlashGS [17] employs an exact intersection algorithm to remove overlapped unnecessary Gaussians on the pre-processing stage, while gsplat [18, 50] supports a CUDA-accelerated differentiable rasterization library for 3DGS. Grendel [53] addresses the computational challenges that arise from dynamic variation in the distribution, shape, color, opacity, and density of Gaussians throughout the training process by implementing a distributed system involving multiple GPUs [7, 25, 29, 44]. By using mixed parallelism and spatial locality of 3DGS, Grendel tackles the issue of dynamic load imbalance. However, we focus on the load imbalance within SMs of the individual GPU and implement Gaussian-wise parallelism at the CUDA rendering level.

4. Approach

In order to address the load imbalance issues across SMs, tiles and training stages mentioned above (in Section 1), we introduce Balanced 3DGS, a Gaussian-wise parallelism rendering with fine-grained tiling approach on 3DGS training. The key of this approach is how to schedule the workloads among different SMs considering the skewed distribution of Gaussians among different image tiles, so that we can achieve an optimal utilization in Gaussian rendering. Besides, it is worth noting that this is a solution without any precision loss.

4.1. Inter-Block Dynamic Workload Distribution

If image tiles are mapped to thread blocks (SMs) in a static method, severe imbalance in Gaussian numbers in different image tile lead to severe load imbalance: some thread blocks will finish their jobs early, while we have to wait until the last thread block with the heaviest workload to finish, and this causes obvious overall performance drop and great compute resources waste.

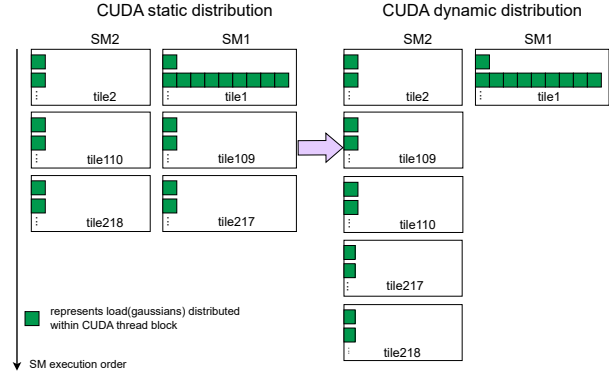


Figure 2. CUDA SM load distribution diagram.

To solve this, we use a dynamic task mapping (distribution) method: 1) tasks of all tiles are collected into a task pool; 2) all thread blocks will get their initial task first; 3) once a thread block finishes its current work, it will immediately fetch next tile from the task pool and run it; 4) all tasks are fetched by thread blocks in such a dynamic method(Algorithm 1). In this way, some thread blocks can focus on a small number of (mostly one) tile(s) with large workloads, while some blocks can deal with many tiles with small workload, thus avoiding idle SMs due to imbalanced workload distribution. Fig. 2 shows an example of SM workload difference between static and dynamic workload distribution.

4.2. Gaussian-Wise Parallel Rendering

Currently, one thread is responsible for processing workloads of one pixel. And the naive render kernel uses pixel-level parallelism, while processes Gaussians in serial. But even inside an image tile where pixels share the same Gaussian group, the actual workloads of different pixels may vary a lot. Because if some of the pixels inside a tile finish their render process in a specific Gaussian, they don't have to iterate over the remaining ones. We call this "early stop". Early stops may cause large variance among workloads of pixels inside a tile. Thus, simply mapping pixels to threads will lead to load imbalance among threads inside a warp. Considering that threads inside a warp run in a SIMT manner, this imbalance also causes a great performance drop.

Accordingly, we propose a warp-collaboration method. All threads inside the same warp will collaborate to process one single pixel by doing Gaussian-wise parallelism to avoid workload divergence inside a warp. In this method, the 32 pixels processed in parallel by a warp in the naive method will be processed in serial. In conclusion, we replace pixel-wise parallelism with Gaussian-wise parallelism to reduce workload divergence inside a warp (Algorithm 2).

In fact, there is dependency in the calculation of different Gaussians of a pixel, as revealed in above Equation 4. Since

Algorithm 1 Inter-Block Dynamic Load Balancing Render Computations

Input: point_xy_image(XY), point_list(PL), conic_opacity(CO), features(F), depths(D)

Output: out_alpha(OA), out_color(OC), out_depth(OD)

```

1: function DYNAMICALLOCATERENDERCUDA(total_tiles, next_tile)
2:   while true do
3:     Synchronize block
4:     if thread_idx == 0 then
5:       my_tile_id ← atomicAdd(next_tile, 1)
6:     end if
7:     Synchronize block
8:     if my_tile_id > total_tiles then
9:       return
10:    end if
11:    Initialize local variables c(color), w(weight), d(depth), t
12:    Load XY, PL, CO to share memory
13:    for j in all gaussians do
14:      BlendInOrder(XY, PL, CO, F, D, c, w, d, t, j)    ▷ Pixel Wise
15:    Parallel
16:      OA, OC, OD ← WriteOutputs(c, w, d, t)
17:    end while
18:  end function
19:
20: function KERNELLAUNCH
21:   total_tiles ← grid.x × grid.y × grid.z, each block deal with 128
22:   next_tile ← 0
23:   max_hw_resource ← 108 (A100 SM) × 16 (16 blocks with 4
24:   dynamicAllocateRenderCUDA<<<<
25:   max_hw_resource, block >>>(total_tiles, next_tile)
26: end function
  
```

we process Gaussians in 32-way parallelism, we need to do one more prefix multiplication operation to assure each Gaussian obtains all results from its precursors inside the 32-size Gaussian group¹. Fig. 3 shows the difference in warp-level pixel-wise parallelism and warp-level Gaussian-wise parallelism.

4.3. Fine-Grained Combined Load Balancing

The two load balancing methods among thread blocks and threads are orthogonal. We can combine them for better performance. Before that, we find that the image tiling size has a significant influence on the load balance, as well as the overall performance. Here the "tiling size" refers to the number of pixels that are assigned to a single thread block.²

Here we use A100 GPU cards to demonstrate why tiling size has a significant influence on the performance. We assume that one thread block contains 128 threads for the simplicity of analysis. A100 has 108 stream multiprocessors (SMs), and each SM can schedule 64 warps (or 16

¹Detailed Implementation See Algorithm 6 line 12 to line 17.

²We define that the pixel block used in the pre-processing calculation is referred to as "patch", and the pixel block utilized by the thread block in the render calculation is named as "tile".

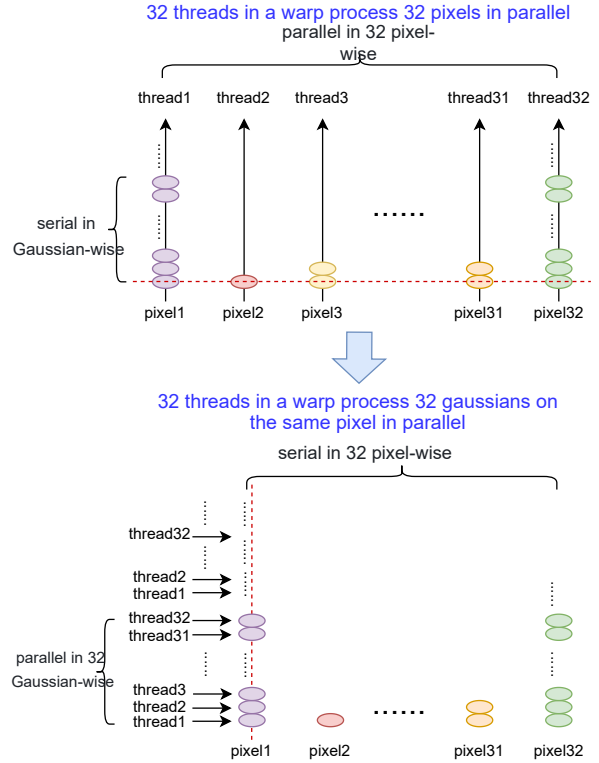


Figure 3. Comparison between pixel-wise parallelism and Gaussian-wise parallelism.

Algorithm 2 Gaussian-Wise Parallel Render Computations

Input: point_xy_image(XY), point_list(PL), conic_opacity(CO), features(F), depths(D)

Output: out_alpha(OA), out_color(OC), out_depth(OD)

```

1: function GAUSSIANPARALLELRENDERCUDA
2:   Initialize local variables c(color), w(weight), d(depth), t, w_t
3:   Load XY, PL, CO to share memory
4:   for p in 32 pixels do    ▷ 32 Pixel Wise Serial
5:     for j = lane_id; j < all gaussians; j += 32 do
6:       BlendParallel(XY, PL, CO, F, D, c, w, d, t, j, p, w_t)    ▷ 32
7:     Gaussians Wise Parallel
8:     InitNext32GaussiansWithLastGaussian(w_t)
9:   end for
10:  OA, OC, OD ← WriteOutputs(c, w, d, t)
11: end function
12:
13: function KERNELLAUNCH
14:   gaussianParallelRenderCUDA<<<< grid, block >>>
15: end function
  
```

blocks with 4 warps in a block) at the same time. Therefore, one wave³ includes as many as $16 \times 108 = 1728$ thread blocks. The original method uses one thread block to deal with one tile with pixel size 16×8 . Considering an image

³A wave refers to a group of thread blocks that are executed concurrently. more waves usually mean more work distribution units, and better flexibility.

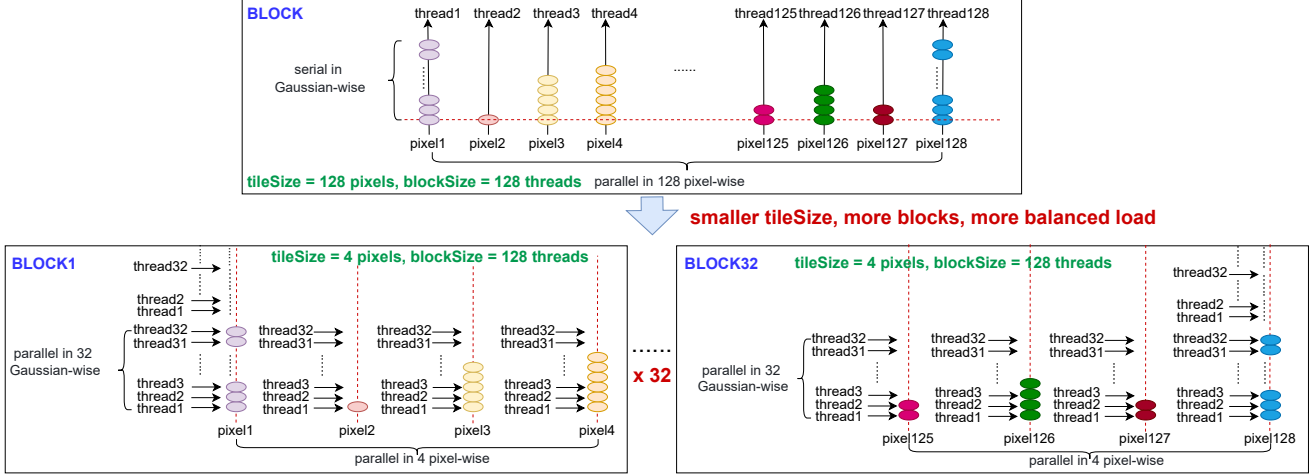


Figure 4. Comparison between pixel-wise parallelism and Gaussian-wise parallelism.

with 960×540 pixels, we can launch $\lceil 960/16 \rceil * \lceil 540/8 \rceil = 4080$ thread blocks, which means there are only $4080/1728 = 2.36$ waves in the render kernel. Load imbalance among tiles may be significant, and we need much larger waves to assure that light-workload tiles workload can accumulate to be comparable to possible extreme heavy-workload tiles.

To solve this, we use a smaller tile size assigned to one thread block (Algorithm 3). Specifically, the patch size before rendering kernel and thread size inside a thread block both remain 16×8 , but we use one thread block to deal with a 4-pixel pattern instead of a 128-pixel patch. This will bring 32x more assignable task groups (Algorithm 3 line 23), therefore, the load balance among blocks is feasible. In the naive render kernel, the Gaussians of a 128-size patch only need to be loaded into shared memory of a block once; since now we use a block to deal with 4 pixels, those Gaussians will be loaded into shared memory by corresponding thread blocks many more times (Algorithm 3 line 13). The tile size of workload distribution is obviously a trade-off between load balance and memory load efficiency. But the Fig. 5 (Gaussians distribution) and our experiments show that addressing load imbalance will bring much more performance benefits.

After using a smaller task distribution size for blocks, we can directly combine the two load-balancing methods introduced in Section 4.1 and Section 4.2. Fig. 4 shows our combined load balancing methods.

4.4. Self-Adaptive Kernel Selection Strategy

The initial data for 3D Gaussian Splitting model training mostly comes from processed LiDAR sparse SfM point cloud data. The trained data features in different training steps vary a lot. The Gaussians of a tile is the key metric of load balance. Fig. 5 shows how Gaussians distribution per block/thread changes as the training goes. In the begin-

Algorithm 3 Fine-Grained Load Balancing Render Computations

Input: point_xy_image(XY), point_list(PL), conic_opacity(CO), features(F), depths(D)

Output: out_alpha(OA), out_color(OC), out_depth(OD)

```

1: function FINEGRAINEDLOADBALANCINGRENDER(total_tiles,
next_tile)
2:   while true do
3:     Synchronize block
4:     if thread_idx == 0 then
5:       my_tile_id ← atomicAdd(next_tile, 1)
6:     end if
7:     Synchronize block
8:     if my_tile_id > total_tiles then
9:       return
10:    end if
11:    Map warp 0, 1, 2, 3 to pixel 0, 1, 2, 3 respectively
12:    Initialize local variables c(color), w(weight), d(depth), t, w.t
13:    Load XY, PL, CO to share memory
14:    for j = lane_id; j < all_gaussians; j += 32 do
15:      BlendParallel(XY, PL, CO, F, D, c, w, d, t, j, w.t)      ▷ 32
16:    Gaussians Wise Parallel
17:    InitNext32GaussiansWithLastGaussian(w.t)
18:  end for
19:  OA, OC, OD ← WriteOutputs(c, w, d, t)
20: end function
21:
22: function KERNELLAUNCH
23:   total_tiles ← grid.x × grid.y × grid.z × 32, each block deals with
4 pixels
24:   next_tile ← 0
25:   max_hw_resource ← 108 (A100 SM) × 16 (16 blocks with 4
warps in a block)
26:   fineGrainedLoadBalancingRender<<<<
max_hw_resource, block >>>>(total_tiles, next_tile)
27: end function

```

ning of the training, the number of Gaussians on different blocks/threads has a large difference, and some extreme-scale blocks/threads, if not processed properly, may lead to

significant performance drop. In this case, we should use our proposed combined load balance optimizations. However, as the training continues, the imbalance in Gaussian number gets better. As we can see from Fig. 5, after some iterations of training, the maximum Gaussian number decreases significantly, and their distribution becomes more concentrated. In this case, still using our load balancing optimizations will not bring much performance benefits; besides, as we introduced above, our optimizations can cause extra overhead (warp-level reduction in Section 4.2 and block-level redundant memory load in Section 4.3). Based on those observations, we should give up those optimizations when the data is already in good balance. Naturally, how to tell whether the data is in good balance, and accordingly choosing the best kernel is key for optimal performance.

Unlike traditional neural network training, a fixed render kernel cannot guarantee balanced workloads in 3DGS training process, so an experiment-based self-adaptive kernel selection strategy is needed, which can avoid manually choosing possible metrics for measuring the data balance, and better reflect the ground truth.

Fig. 6 demonstrates our training process. We start with our workload-balancing kernels. Every 1000 iterations, we compare the performance of two kernels by running two kernels with current data separately. If the workload-balancing kernel has worse performance, we assume that the data is already in good balance, so the remaining training will use the original kernel. For the original kernel, we also make some memory-access optimizations, as can be seen in Section 5.2.2.

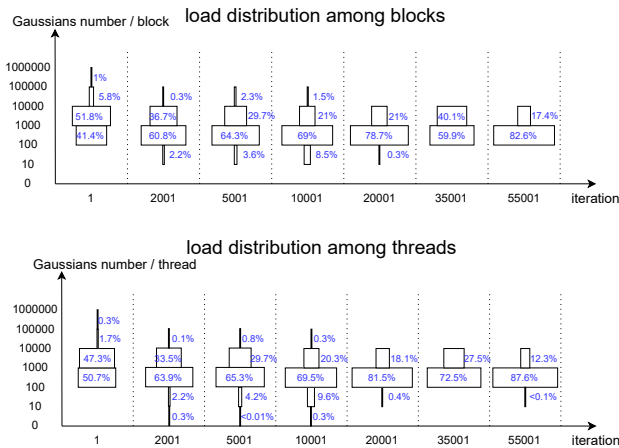


Figure 5. Gaussians load distribution among blocks and threads at different training iterations.

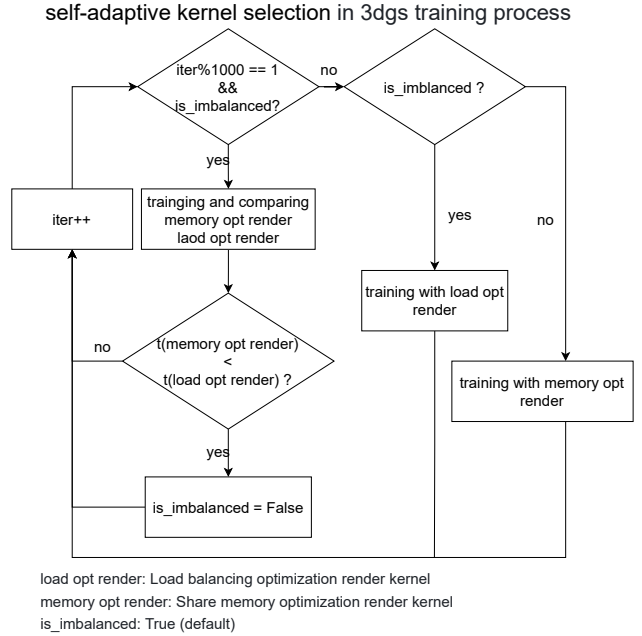


Figure 6. Schematic diagram of self-adaptive kernel selection strategy

5. Experiments

5.1. Experimental Setup

In this experiment, we utilize NVIDIA’s Nsight series performance analysis tools, specifically Nsight Compute [39], which focuses on analyzing the execution efficiency of specific CUDA kernels, such as the optimized renderCUDA kernel discussed in this paper. The hardware platform is based on the NVIDIA A100 SMX4 80GB, and the software environment utilizes PyTorch 1.13 with CUDA version 11.8. The dataset is derived from the internal 3D Gaussian model training smoke test dataset of Li Auto. The rasterization module during the 3D Gaussian training process is the main focus of the work, which is primarily based on the open-source project Street Gaussians [47]. The specific experiment mainly aims to evaluate the execution time of the forward renderCUDA kernel in the rasterization module under different optimization methods.

5.2. Experiment Processes and Result analysis

5.2.1 Load Balancing Optimization Experiment

To better evaluate the forward render kernel, we selected the data from the first iteration of the training process as the evaluation target. The size of the 2D pixel plane is (960, 540), and the preprocessing patch size is (16, 8), we sequentially applied the optimization methods mentioned above while utilizing the Nsight Compute tool. The test results are shown in Table 1.

Naive Experiment. First, we conduct a naive experiment. Based on the CUDA static distribution method, image pixel size and patch size, the kernel launch configuration can be easily calculated, that is, $grid = (\lceil 960/16 \rceil, \lceil 540/8 \rceil, 1)$, $block = (16, 8, 1)$ (Algorithm 4 line 11).

Algorithm 4 Naive Render Computations

```

Input: point_xy_image(XY), point_list(PL), conic_opacity(CO), features(F), depths(D)
Output: out.alpha(OA), out.color(OC), out.depth(OD)
1: function RENDERCUDA
2:   Initialize local variables c(color), w(weight), d(depth), t
3:   Load XY, PL, CO to share memory
4:   for j in all gaussians do
5:     BlendInOrder(XY,PL,CO,F,D,c,w,d,t,j) ▷ Pixel Wise Parallel
6:   end for
7:   OA, OC, OD ← WriteOutputs(c, w, d, t)
8: end function
9:
10: function KERNELLAUNCH
11:   renderCUDA<<< grid, block >>>
12: end function

```

As can be seen from Table 1 (a), the time of naive render kernel is 125.5ms, and only 22.6% occupancy is achieved, which is far from the upper limit of theoretical occupancy, mainly due to the load imbalance at CUDA level.

Inter-Block Dynamic Workload Distribution Experiment. In the case of dynamic loading distribution, the kernel launch configuration is calculated based on hardware compute resources(Algorithm 1 line 23). To obtain the current processing tile_id, the total workload quantity total_tiles and the current processing tile_id need to be passed as parameters to the kernel(Algorithm 1 line 1, 21, 22, 24). Additionally, a loop for workload distribution logic must be included within the kernel function to achieve dynamic load balancing scheduling(Algorithm 1 line 1, 21, 22, 24).

As shown in Table 1 (b), the kernel execution time has been reduced to 120ms, only a 4.6% improvement compared to the naive case, and the achieved occupancy is just 19.82%, showing a significant gap compared to the theoretical occupancy limit of 75%. So the load imbalance problem still exists. As explained in 4.3, the dynamic distribution capability is not strong enough to comprehensively address the load imbalance issues if the tile size(16, 8) remains unchanged.

Gaussian-Wise Parallel Rendering Experiment. The number of Gaussians processed by different CUDA threads varies from hundreds to hundreds of thousands shown in Fig. 5. Thus We conduct warp-collaboration experiment, which replaces Pixel-wise parallelism with Gaussian-wise parallelism to reduce workload divergence inside a warp.

The kernel launch configuration is the same as naive experiment(Algorithm 2).

As shown in 1 (c), the kernel execution time has decreased to 107.36ms, representing a 16.8% performance improvement compared to the naive one. However, there is still a significant gap between achieved occupancy and theoretical occupancy, and the load imbalance issues persist.

Fine-Grained Combined Load Balancing Experiment. To further eliminate the load imbalance issues, we combine inter-block dynamic workload distribution and Gaussian-wise parallel rendering approaches with fine-grained pixel tile. Specifically, the size of patch and thread block remains (16, 8) (Algorithm 3 line 26), but we use one thread block to deal with a 4-pixel tile instead of a 128-pixel tile(Algorithm 3 line 23). Thus the total task tiles are increased by 32x and each warp focuses on one pixel(Algorithm 3 line 11 and line 23). Although the memory access overhead will also increase by 32x(Algorithm 3 line 13), it accounts for a small proportion in severe load imbalance scenarios. In this way, we can comprehensively address the load imbalance issues among warps and blocks.

As shown in 1 (d), the kernel execution time has been reduced to 16.69ms, 7.52X faster than the naive version. Additionally, the achieved occupancy is now very close to the theoretical occupancy, indicating the load imbalance issues among warps and blocks have been completely solved. This time, the achieved occupancy is mainly limited by the number of required registers, which is highly related to algorithm logic.

5.2.2 Self-Adaptive Kernel Selection Experiment

As 3DGS training progresses, the training data transitions from an initially unbalanced distribution to a more balanced state as shown in Fig. 5. Based on the naive render kernel, we also make some memory access optimization. Specifically, we put features and depths to share memory too (refer to Algorithm 4 line 3). Although this optimization has little effect in load imbalance situations at training initial stage due to the relatively small proportion of memory access overhead, with the training process going, the effect of shared-memory access optimization is increasingly evident owing to the progressively balanced load.

Next, we collect performance data during the training process using both combined load-balancing render kernel and shared-memory optimized render kernel, as shown in Fig. 7. It can be observed that from 0 to 2000 training steps, the combined load-balancing kernel performs much better than the shared-memory optimized kernel. After 2000 steps, the combined load-balancing kernel exhibits a

Table 1. Experiments Comparison

Experiments	Time(ms)	Theoretical Occupancy(%)	Achieved Occupancy(%)	Occupancy Limiters
Native	125.50	100.00	22.60	Load Imbalance
Inter-Block Dynamic Workload Distribution	120.00 (1.05x \uparrow)	75.00	19.82	Load Imbalance
Gaussian-Wise Parallel Rendering	107.36 (1.17x \uparrow)	31.25	18.85	Load Imbalance
Fine-Grained Combined Load Balancing	16.69 (7.52x \uparrow)	62.50	55.02	Used Registers Number

slightly inferior performance. The primary reason for this decline is that as the training process iterates, the distribution of Gaussians approaches a balanced state, in which scenario fine-grained combined load balancing optimization causes extra overhead, namely warp-level reduction and block-level redundant memory load described in Section 4.4. It’s important to note that, in a load balanced state, the memory access overhead is non-negligible. Additionally, the increased usage of registers also limits the upper bound of warp occupancy. These factors together result in worse performance for the combined load-balancing kernel.

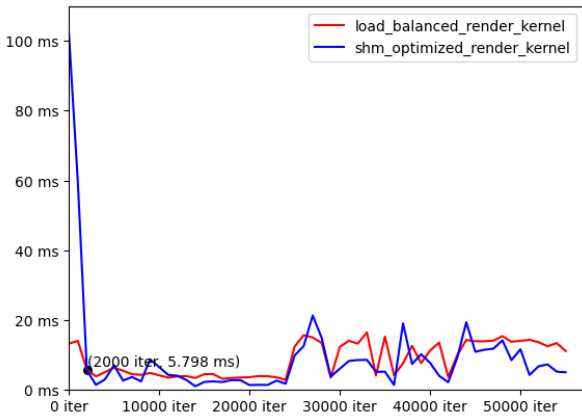


Figure 7. Optimized render kernel performance during 3DGS training process.

Given that the data workload distribution during the 3D-Gaussian model training process transitions from severe imbalance in the initial stages to a more balanced state later on, shown in Fig. 5. We propose an experiment-based self-adaptive kernel selection strategy during the training process to accelerate training efficiency. Specifically, during the initial stage of the model training, we choose fine-grained combined load balancing render kernel by default. Then, after every 1000 (which can be configured before training start) iterations, we compare the performance of these two kernels (fine-grained combined load balancing render kernel and the shared-memory optimized render kernel), until a performance inflection point is reached, which occurs when the distribution of Gaussians becomes balanced. After this point, subsequent iterations will select the

shared-memory optimized render kernel.

The e2e performances of 3DGS training with self-adaptive kernel selection strategy and naive 3DGS training are shown in Fig. 8. It can be easily obtained that from the beginning of training to the inflection point, compared to the naive version, the optimized training speeds up by 19.6%; From the inflection point to the end of model training, the optimized training speeds up by 7.9%. Overall, the optimized training speeds up by 8.5%.

5.3. Discussion and Limitations

Through our experiments, we have completely resolved the problem of poor rendering performance attributed to load imbalance during 3DGS training initial stage, and the more extreme the load imbalance scenarios are, the better the performance will be. Although our current method has also shown certain effectiveness in 3DGS multiple GPUs training, a systematic analysis from the perspective of 3DGS multiple GPUs training has not been conducted yet. In the next step, we will combine dynamic load balancing technology of 3DGS multiple GPUs distributed training [53] with our approaches to further enhance 3DGS training efficiency in large-model or large-scale scene reconstruction scenarios.

6. Conclusion

We introduce Balanced 3DGS, a Gaussian-wise parallelism rendering with fine-grained tiling approach in 3DGS training process, perfectly solving load-imbalance issue. In load imbalance scenarios, the forward renderCUDA kernel performance can be significantly enhanced through inter-block dynamic workload distribution, Gaussian-wise parallel rendering and fine-grained combined load balancing techniques. At the same time, 3DGS can self-adaptively choose the best renderCUDA kernel during the training process based on different load-balance situations, which effectively improves training efficiency.

References

[1] Muhammad Salman Ali, Maryam Qamar, Sung-Ho Bae, and Enzo Tartaglione. Trimming the fat: Efficient compression of 3d gaussian splats through pruning. *arXiv preprint arXiv:2406.18214*, 2024. 1, 3

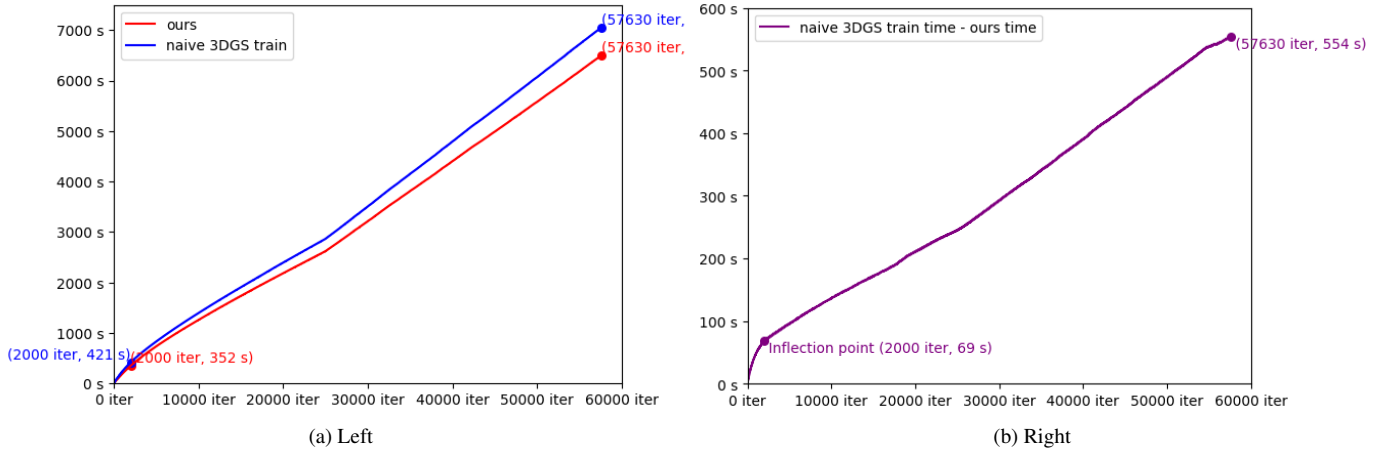


Figure 8. (a) Left: 3DGS e2e training time (naive vs ours); (b) Right: 3DGS e2e training time Difference (naive - ours)

- [2] Yanqi Bao, Tianyu Ding, Jing Huo, Yaoli Liu, Yuxin Li, Wenbin Li, Yang Gao, and Jiebo Luo. 3d gaussian splatting: Survey, technologies, challenges, and opportunities. *arXiv preprint arXiv:2407.17418*, 2024. 1, 3
- [3] Chris Buehler, Michael Bosse, Leonard McMillan, Steven Gortler, and Michael Cohen. Unstructured lumigraph rendering. In *Proceedings of the 28th annual conference on Computer graphics and interactive techniques*, pages 425–432, 2001. 3
- [4] Ang Cao and Justin Johnson. Hexplane: A fast representation for dynamic scenes. In *Proceedings of the IEEE/CVF Conference on Computer Vision and Pattern Recognition*, pages 130–141, 2023. 1, 3
- [5] Gaurav Chaurasia, Sylvain Duchene, Olga Sorkine-Hornung, and George Drettakis. Depth synthesis and local warps for plausible image-based navigation. *ACM transactions on graphics (TOG)*, 32(3):1–12, 2013. 3
- [6] Guikun Chen and Wenguan Wang. A survey on 3d gaussian splatting. *arXiv preprint arXiv:2401.01339*, 2024. 1, 3
- [7] Yu Chen and Gim Hee Lee. Dogs: Distributed-oriented gaussian splatting for large-scale 3d reconstruction via gaussian consensus. In *The Thirty-eighth Annual Conference on Neural Information Processing Systems*, 2024. 4
- [8] Yihang Chen, Qianyi Wu, Weiyao Lin, Mehrtash Harandi, and Jianfei Cai. Hac: Hash-grid assisted context for 3d gaussian splatting compression. In *European Conference on Computer Vision*, pages 422–438. Springer, 2025. 1, 3
- [9] Yuedong Chen, Haofei Xu, Chuanxia Zheng, Bohan Zhuang, Marc Pollefeys, Andreas Geiger, Tat-Jen Cham, and Jianfei Cai. Mvsplat: Efficient 3d gaussian splatting from sparse multi-view images. In *European Conference on Computer Vision*, pages 370–386. Springer, 2025. 3
- [10] Kai Cheng, Xiaoxiao Long, Kaizhi Yang, Yao Yao, Wei Yin, Yuexin Ma, Wenping Wang, and Xuejin Chen. Gaussianpro: 3d gaussian splatting with progressive propagation. In *Forty-first International Conference on Machine Learning*, 2024. 3
- [11] Ziang Cheng, Hongdong Li, Yuta Asano, Yinqiang Zheng, and Imari Sato. Multi-view 3d reconstruction of a texture-less smooth surface of unknown generic reflectance. In *Proceedings of the IEEE/CVF Conference on Computer Vision and Pattern Recognition*, pages 16226–16235, 2021. 3
- [12] Yuanxing Duan, Fangyin Wei, Qiyu Dai, Yuhang He, Wenzheng Chen, and Baoquan Chen. 4d-rotor gaussian splatting: towards efficient novel view synthesis for dynamic scenes. In *ACM SIGGRAPH 2024 Conference Papers*, pages 1–11, 2024. 3
- [13] Sankeerth Durvasula, Adrian Zhao, Fan Chen, Ruofan Liang, Pawan Kumar Sanjaya, and Nandita Vijaykumar. Distwar: Fast differentiable rendering on raster-based rendering pipelines. *arXiv preprint arXiv:2401.05345*, 2023. 1, 3, 4
- [14] Martin Eisemann, Bert De Decker, Marcus Magnor, Philippe Bekaert, Edilson De Aguiar, Naveed Ahmed, Christian Theobalt, and Anita Sellent. Floating textures. In *Computer graphics forum*, volume 27, pages 409–418. Wiley Online Library, 2008. 3
- [15] Guangchi Fang and Bing Wang. Mini-splatting: Representing scenes with a constrained number of gaussians. *arXiv preprint arXiv:2403.14166*, 2024. 1, 4
- [16] Ben Fei, Jingyi Xu, Rui Zhang, Qingyuan Zhou, Weidong Yang, and Ying He. 3d gaussian splatting as new era: A survey. *IEEE Transactions on Visualization and Computer Graphics*, page 1–20, 2024. 1, 3
- [17] Guofeng Feng, Siyan Chen, Rong Fu, Zimu Liao, Yi Wang, Tao Liu, Zhilin Pei, Hengjie Li, Xingcheng Zhang, and Bo Dai. Flashgs: Efficient 3d gaussian splatting for large-scale and high-resolution rendering. *arXiv preprint arXiv:2408.07967*, 2024. 4
- [18] Sharath Girish, Kamal Gupta, and Abhinav Shrivastava. Eagles: Efficient accelerated 3d gaussians with lightweight encodings. In *European Conference on Computer Vision*, pages 54–71. Springer, 2025. 1, 4
- [19] Michael Goesele, Noah Snavely, Brian Curless, Hugues Hoppe, and Steven M Seitz. Multi-view stereo for community photo collections. In *2007 IEEE 11th International Conference on Computer Vision*, pages 1–8. IEEE, 2007. 3

- [20] Steven J Gortler, Radek Grzeszczuk, Richard Szeliski, and Michael F Cohen. The lumigraph. In *Seminal Graphics Papers: Pushing the Boundaries, Volume 2*, pages 453–464, 2023. 3
- [21] Peter Hedman, Julien Philip, True Price, Jan-Michael Frahm, George Drettakis, and Gabriel Brostow. Deep blending for free-viewpoint image-based rendering. *ACM Transactions on Graphics (ToG)*, 37(6):1–15, 2018. 3
- [22] Lukas Höllein, Aljaž Božič, Michael Zollhöfer, and Matthias Nießner. 3dgs-lm: Faster gaussian-splatting optimization with levenberg-marquardt. *arXiv preprint arXiv:2409.12892*, 2024. 1, 3
- [23] Rasmus Jensen, Anders Dahl, George Vogiatzis, Engin Tola, and Henrik Aanaes. Large scale multi-view stereopsis evaluation. In *Proceedings of the IEEE Conference on Computer Vision and Pattern Recognition (CVPR)*, June 2014. 3
- [24] Bernhard Kerbl, Georgios Kopanas, Thomas Leimkühler, and George Drettakis. 3d gaussian splatting for real-time radiance field rendering. *ACM Trans. Graph.*, 42(4):139–1, 2023. 1, 2, 3
- [25] Bernhard Kerbl, Andreas Meuleman, Georgios Kopanas, Michael Wimmer, Alexandre Lanvin, and George Drettakis. A hierarchical 3d gaussian representation for real-time rendering of very large datasets. *ACM Transactions on Graphics (TOG)*, 43(4):1–15, 2024. 4
- [26] Georgios Kopanas, Julien Philip, Thomas Leimkühler, and George Drettakis. Point-based neural rendering with per-view optimization. In *Computer Graphics Forum*, volume 40, pages 29–43. Wiley Online Library, 2021. 3
- [27] Joo Chan Lee, Daniel Rho, Xiangyu Sun, Jong Hwan Ko, and Eunbyung Park. Compact 3d gaussian representation for radiance field. In *Proceedings of the IEEE/CVF Conference on Computer Vision and Pattern Recognition*, pages 21719–21728, 2024. 1, 3
- [28] Marc Levoy and Pat Hanrahan. Light field rendering. In *Seminal Graphics Papers: Pushing the Boundaries, Volume 2*, pages 441–452, 2023. 3
- [29] Bingling Li, Shengyi Chen, Luchao Wang, Kaimin Liao, Si-jie Yan, and Yuanjun Xiong. Retinags: Scalable training for dense scene rendering with billion-scale 3d gaussians. *arXiv preprint arXiv:2406.11836*, 2024. 4
- [30] Jiahe Li, Jiawei Zhang, Xiao Bai, Jin Zheng, Xin Ning, Jun Zhou, and Lin Gu. Dngaussian: Optimizing sparse-view 3d gaussian radiance fields with global-local depth normalization. In *Proceedings of the IEEE/CVF Conference on Computer Vision and Pattern Recognition*, pages 20775–20785, 2024. 1, 3
- [31] Yanyan Li, Chenyu Lyu, Yan Di, Guangyao Zhai, Gim Hee Lee, and Federico Tombari. Geogaussian: Geometry-aware gaussian splatting for scene rendering. In *European Conference on Computer Vision*, pages 441–457. Springer, 2025. 1, 3
- [32] Tao Lu, Mulin Yu, Linning Xu, Yuanbo Xiangli, Limin Wang, Dahua Lin, and Bo Dai. Scaffold-gs: Structured 3d gaussians for view-adaptive rendering. In *Proceedings of the IEEE/CVF Conference on Computer Vision and Pattern Recognition*, pages 20654–20664, 2024. 3
- [33] Jonathon Luiten, Georgios Kopanas, Bastian Leibe, and Deva Ramanan. Dynamic 3d gaussians: Tracking by persistent dynamic view synthesis. *arXiv preprint arXiv:2308.09713*, 2023. 1, 3
- [34] Shengjie Ma, Yanlin Weng, Tianjia Shao, and Kun Zhou. 3d gaussian blendshapes for head avatar animation. In *ACM SIGGRAPH 2024 Conference Papers*, pages 1–10, 2024. 3
- [35] Saswat Subhajyoti Mallick, Rahul Goel, Bernhard Kerbl, Markus Steinberger, Francisco Vicente Carrasco, and Fernando De La Torre. Taming 3dgs: High-quality radiance fields with limited resources. In *SIGGRAPH Asia 2024 Conference Papers*, pages 1–11, 2024. 1, 4
- [36] Ben Mildenhall, Pratul P Srinivasan, Matthew Tancik, Jonathan T Barron, Ravi Ramamoorthi, and Ren Ng. Nerf: Representing scenes as neural radiance fields for view synthesis. *Communications of the ACM*, 65(1):99–106, 2021. 3
- [37] KL Navaneet, Kossar Pourahmadi Meibodi, Soroush Abbasi Koohpayegani, and Hamed Pirsiavash. Compgs: Smaller and faster gaussian splatting with vector quantization. In *European Conference on Computer Vision*, pages 330–349. Springer, 2025. 1, 3
- [38] Simon Niedermayr, Josef Stumpfegger, and Rüdiger Westermann. Compressed 3d gaussian splatting for accelerated novel view synthesis. In *Proceedings of the IEEE/CVF Conference on Computer Vision and Pattern Recognition*, pages 10349–10358, 2024. 3
- [39] NVIDIA. Nsight compute. <https://docs.nvidia.com/nsight-compute/ProfilingGuide/index.html#metrics-hw-model>, 2024. 7
- [40] Panagiotis Papantonakis, Georgios Kopanas, Bernhard Kerbl, Alexandre Lanvin, and George Drettakis. Reducing the memory footprint of 3d gaussian splatting. *Proceedings of the ACM on Computer Graphics and Interactive Techniques*, 7(1):1–17, 2024. 3
- [41] Zhexi Peng, Tianjia Shao, Yong Liu, Jingke Zhou, Yin Yang, Jingdong Wang, and Kun Zhou. Rtg-slam: Real-time 3d reconstruction at scale using gaussian splatting. In *ACM SIGGRAPH 2024 Conference Papers*, pages 1–11, 2024. 3
- [42] Lukas Radl, Michael Steiner, Mathias Parger, Alexander Weinrauch, Bernhard Kerbl, and Markus Steinberger. Stopthepop: Sorted gaussian splatting for view-consistent real-time rendering. *ACM Transactions on Graphics (TOG)*, 43(4):1–17, 2024. 3
- [43] Johannes L. Schönberger and Jan-Michael Frahm. Structure-from-motion revisited. In *2016 IEEE Conference on Computer Vision and Pattern Recognition (CVPR)*, pages 4104–4113, 2016. 3
- [44] Kaiwen Song, Xiaoyi Zeng, Chenqu Ren, and Juyong Zhang. City-on-web: Real-time neural rendering of large-scale scenes on the web. In *European Conference on Computer Vision*, pages 385–402. Springer, 2025. 4
- [45] Jiakai Sun, Han Jiao, Guangyuan Li, Zhanjie Zhang, Lei Zhao, and Wei Xing. 3dgstream: On-the-fly training of 3d gaussians for efficient streaming of photo-realistic free-viewpoint videos. In *Proceedings of the IEEE/CVF Conference on Computer Vision and Pattern Recognition*, pages 20675–20685, 2024. 1, 3

- [46] Tianyi Xie, Zeshun Zong, Yuxing Qiu, Xuan Li, Yutao Feng, Yin Yang, and Chenfanfu Jiang. Physgaussian: Physics-integrated 3d gaussians for generative dynamics. In *Proceedings of the IEEE/CVF Conference on Computer Vision and Pattern Recognition*, pages 4389–4398, 2024. 1, 3
- [47] Yunzhi Yan, Haotong Lin, Chenxu Zhou, Weijie Wang, Haiyang Sun, Kun Zhan, Xianpeng Lang, Xiaowei Zhou, and Sida Peng. Street gaussians for modeling dynamic urban scenes. In *ECCV*, 2024. 7
- [48] Zhiwen Yan, Weng Fei Low, Yu Chen, and Gim Hee Lee. Multi-scale 3d gaussian splatting for anti-aliased rendering. In *Proceedings of the IEEE/CVF Conference on Computer Vision and Pattern Recognition*, pages 20923–20931, 2024. 3
- [49] Keyang Ye, Qiming Hou, and Kun Zhou. 3d gaussian splatting with deferred reflection. In *ACM SIGGRAPH 2024 Conference Papers*, pages 1–10, 2024. 3
- [50] Vickie Ye, Ruilong Li, Justin Kerr, Matias Turkulainen, Brent Yi, Zhuoyang Pan, Otto Seiskari, Jianbo Ye, Jeffrey Hu, Matthew Tancik, et al. gsplat: An open-source library for gaussian splatting. *arXiv preprint arXiv:2409.06765*, 2024. 1, 4
- [51] Zehao Yu, Anpei Chen, Binbin Huang, Torsten Sattler, and Andreas Geiger. Mip-splatting: Alias-free 3d gaussian splatting. In *Proceedings of the IEEE/CVF Conference on Computer Vision and Pattern Recognition*, pages 19447–19456, 2024. 3
- [52] Jiahui Zhang, Fangneng Zhan, Muyu Xu, Shijian Lu, and Eric Xing. Fregs: 3d gaussian splatting with progressive frequency regularization. In *Proceedings of the IEEE/CVF Conference on Computer Vision and Pattern Recognition*, pages 21424–21433, 2024. 3
- [53] Hexu Zhao, Haoyang Weng, Daohan Lu, Ang Li, Jinyang Li, Aurojit Panda, and Saining Xie. On scaling up 3d gaussian splatting training. *arXiv preprint arXiv:2406.18533*, 2024. 1, 4, 9

A. Implementation Details

Algorithm 5 and 6 show the difference of two parallelism methods in warp-level computation. Here we concentrate on the difference of warp-level thread divergency and collaboration, and omit computation details of *power*, *alpha* and *t* in Algorithm 5 and 6.

In pixel-parallelism kernel, one thread gets a pixel (Algorithm 5 line 2), and iterates over all concerned gaussian spheres (Algorithm 5 line 5). For each pixel and each gaussian sphere: after some related computation (Algorithm 5 line 7), if it’s a valid gaussian sphere (Algorithm 5 line 8) and the computation of current pixel has not finished (Algorithm 5 line 12), the thread will update this pixel with related variables (Algorithm 5 line 17). Besides, *t* is a variable in *pixel* we should pay attention to, because each update of *t* depends on the results of calculations of all previous gaussian spheres. When we implement gaussian sphere dimension parallelism, we should also ensure the correctness of *t*.

In our proposed kernel, we use gaussian sphere dimension 32-way parallelism, and pixels are processed in serial (Algorithm 6 line 4). We use warp-level primitives to assure the warp works as a whole in determining execution paths (Algorithm 6 line 13 and line 23). To assure the correct accumulation of *t*, we use warp shuffle primitives (Algorithm 6 line 12-17) to multiply all *alpha* in every precursor threads (Algorithm 6 line 15), and then broadcast the *t* in last thread to all threads as the *t* for next gaussian sphere group (Algorithm 6 line 23). Besides, each *pixel* in each thread now is a partially updated results, so we need to warp-level reduction (Algorithm 6 line 28) to obtain the same result as that in Algorithm 5.

In this way, we implement a gaussian sphere dimension parallelism kernel. Warp naturally runs in SIMT manner, therefore, we can avoid thread divergency by enabling threads inside a warp to run similar workload. Besides, the usage of warp-level primitives assure that intra warp thread communications will not introduce much overhead.

Algorithm 5 detail naive render computations

Input: point_xy_image(XY), point_list(PL), conic_opacity(CO), features(F), depths(D)

Output: out_alpha(OA), out_color(OC), out_depth(OD)

```

1: function RENDERCUDA
2:   pixel = pixels[lane_id]
3:   Initialize local variables c(color), w(weight), d(depth), t
4:   Load XY, PL, CO to share memory
5:   for j = 0; j < gaussians.size() and !finished; j ++ do
6:     Initialize local variables alpha, power, tmp_t
7:     pixelGaussianCompute(XY, PL, CO, j, alpha, power)
8:     if power > 0 or alpha < 1/255 then
9:       continue
10:    end if
11:    tmp_t = t * (1 - alpha)
12:    if tmp_t < 0.0001 then
13:      finished = True
14:      break
15:    end if
16:    t = tmp_t
17:    accumulateToLocalVariables(alpha,tmp_t, F, D, c, w, d)
18:  end for
19:  OA, OC, OD ← WriteOutputs(c, w, d, t)
20: end function

```

Algorithm 6 detail gaussian-wise parallel render computations

Input: point_xy_image(XY), point_list(PL), conic_opacity(CO), features(F), depths(D)

Output: out_alpha(OA), out_color(OC), out_depth(OD)

```
1: function GAUSSIANPARALLELRENDER
2:   Initialize local variables c(color), w(weight), d(depth), t
3:   Load XY, PL, CO to share memory
4:   for p = 0; p < 32; p ++ do
5:     pixel = pixels[p];
6:     for j = lane_id; j < gaussians.size() and !finished; j += 32 do
7:       Initialize local variables alpha, power, tmp_t, one_alpha,
w_c, w_w, w_d
8:       pixelGaussianCompute(XY, PL, CO, j, alpha, one_alpha,
power)
9:       if !_all_sync(power > 0 or alpha < 1/255) then
10:         continue
11:       end if
12:       for offset = 1; offset < 32; offset *= 2 do
13:         v = _shfl_up_sync(one_alpha, offset, 32)
14:         if lane_id % 32 ≥ offset then
15:           one_alpha *= v
16:         end if
17:       end for
18:       tmp_t = t * one_alpha
19:       if !_any_sync(tmp_t < 0.0001) then
20:         finished = True
21:       end if
22:       t = tmp_t
23:       t = _shfl_sync(t, 31)
24:       if valid_gaussian_spheres then
25:         accumulateToLocalVariables(alpha, tmp_t, F, D, w_c,
w_w, w_d)
26:       end if
27:     end for
28:     c, w, d ← warp_reduce(w_c, w_w, w_d)
29:   end for
30:   OA, OC, OD ← WriteOutputs(c, w, d, t)
31: end function
```
